Journal of Chromatography A, 1218 (2011) 1611–1619

Contents lists available at ScienceDirect

Journal of Chromatography A

journal homepage: www.elsevier.com/locate/chroma

Microchip electrospray: Cone-jet stability analysis for water–acetonitrile and water–methanol mobile phases

Stephanie Jung[a], Uwe Effelsberg[b], Ulrich Tallarek[a,*]

[a] Department of Chemistry, Philipps-Universität Marburg, Hans-Meerwein-Strasse, 35032 Marburg, Germany
[b] Agilent Technologies, Hewlett-Packard-Strasse 8, 76337 Waldbronn, Germany

ARTICLE INFO

Article history:
Received 27 November 2010
Received in revised form 14 January 2011
Accepted 17 January 2011
Available online 22 January 2011

Keywords:
Microchip HPLC/ESI-MS
Electrospray modes
Cone-jet stability island
Gradient elution
Bulk conductivity
Organic modifier content
Flow rate effect

ABSTRACT

Changes in mobile phase composition during high performance liquid chromatography (HPLC) gradient elution coupled to mass spectrometry (MS) sensitively affect electrospray operation modes. In this work, we identify the influences of dynamic changes in bulk conductivity on the cone-jet stability island for aqueous acetonitrile and aqueous methanol mobile phases commonly used in reversed-phase HPLC. Bulk conductivities of the mobile phases were varied by adding different amounts of formic acid. A commercial microchip-HPLC/ESI-MS configuration was modified to enable *in situ* electrospray diagnostics by frequency analysis of the microchip emitter current and spray imaging. This approach facilitated the detection of different spray modes together with their onset potentials. The established spray modes are described and the differences in onset potentials and stability regions explained by the physicochemical properties of the electrosprayed liquid.

1. Introduction

Microfluidic devices have become increasingly important in analytical and bioanalytical chemistry [1–6]. They offer the ability to save time, sample amount, and costs by miniaturizing and integrating sample pre-treatment and analysis steps on a microfluidic chip. Micro total analysis systems (μ-TAS) [7] also offer parallelization and automation, ideal for high-throughput screening and proteomic workflows. Among a variety of separation and detection methods [8,9], the combination of high performance liquid chromatography (HPLC) with electrospray ionization (ESI) mass spectrometry (MS) has emerged as the standard analytical method for many applications, from screening of small molecule libraries to peptide and protein identification and structural characterization [10]. Anticipating the trend towards chip-based technologies, efforts to couple microfluidic devices to mass spectrometers started a decade ago [11–13]. ESI – a soft, atmospheric-pressure ionization method for small and large molecules alike, provided they possess polar functionalities that can be protonated or deprotonated – is well suited to microfluidic flow rates and to the aqueous methanol or aqueous acetonitrile-based mobile phases used in reversed-phase (RP) HPLC. There has also been strong interest to bring the chromatographic separation into microchip format, but the difficulties related to generating and maintaining high-pressure liquid flow on the (usually pressure-sensitive) chips and to preparing homogeneous packed beds in the noncylindrical microfluidic channels had to be overcome first [14]. Another challenge for the coupling of chip-based HPLC to ESI-MS was the development of a stable and effective interface with minimal dead volume [15].

Apart from the design and manufacturing of microchips for HPLC/ESI-MS, the operating conditions are also important to their performance. The physical processes involved in the electrospray are complex, and many parameters have been established by trial and error. Today, we have arrived at a better understanding of the ESI mechanism [16], which enables rational choices for the proper conditions in ESI-MS. Electrostatic spraying exhibits a variety of spray morphologies and dynamics [17], depending on a number of parameters related to instrumental design (geometry and wettability of the emitter, distance between emitter and counter electrode, strength and shape of the electrical field) as well as to flow rate and physicochemical properties of the electrosprayed liquid (surface tension, permittivity, viscosity, density, electrical conductivity) [11,18–22]. Although spray morphologies and dynamics depend on the actual experimental conditions, the involved physical and electrohydrodynamic phenomena are transferable between individual systems allowing a comparison between the observed electrospray modes and their related instrument settings. In

* Corresponding author. Tel.: +49 6421 28 25727; fax: +49 6421 28 22124.
E-mail address: tallarek@staff.uni-marburg.de (U. Tallarek).

0021-9673/$ – see front matter © 2011 Elsevier B.V. All rights reserved.
doi:10.1016/j.chroma.2011.01.054

general, microchip emitters demonstrate similar or even better chromatographic performance and comparable ESI-MS sensitivities with respect to nanoelectrospray needles of similar emitter diameters [19,23–25].

Electrospray modes are classified by visual criteria [17,26] and/or by measuring the AC and DC components of the spray current [27–31]. The different spray modes impact sensitivity and precision of the measurement. The targeted spray condition for mass spectrometric analysis is the cone-jet mode, which provides a relatively large and stable current as well as smaller initial droplets, both prerequisites for high sensitivity and precision [16,19]. Choosing the experimental parameters so as to operate in the cone-jet mode throughout the detection duty cycle is desirable, but in conflict with the reality of typical screening applications, where RP-HPLC separation is carried out with steep mobile phase gradients to cover a broad range of analytes in a short analysis time. A gradually changing mobile phase composition implies a dynamic change of the physicochemical properties of the electrosprayed liquid (the eluate from the chip's separation channel), which could result in transitions between different spray modes and alterations in the detected signal. There have been a few attempts to automatically maintain the electrospray in the cone-jet mode by adjusting the voltage based on feedback from spray imaging [22] or spray current measurements [20,32]. Alternatively, the effects of a changing mobile phase composition could be counter-balanced by post-column combination with an inverted mobile phase gradient to provide constant physicochemical properties of the electrosprayed liquid during MS analysis [33,34].

In this work, we analyze the electrospray characteristics of a microchip-HPLC/ESI-MS configuration for formic acid-containing mobile phases of aqueous acetonitrile and aqueous methanol. We study the flow-rate dependence, the influence of water fraction and formic acid content in the mobile phase, and the effect of a gradually changing bulk conductivity of the electrosprayed liquid. The electrospray is monitored with an oscilloscope for frequency analysis of the emitter current's DC and AC components and with a video camera for spray imaging. This approach enables identification of different spray modes as well as the determination of their stability islands depending on the applied voltage and actual mobile phase conditions. We discuss our results in terms of the physicochemical properties of the electrosprayed liquid, particularly its conductivity, and focus on the effects that accompany the gradual variation of solvent volumetric ratios in gradient elution RP-HPLC.

In our previous work [31], we presented and used this modified experimental setup to identify dynamic changes in bulk conductivity during RP-HPLC as a major source for spray mode changes and instabilities observed in ESI-MS. Importantly, in that previous work experimental data were complemented by computational fluid dynamics simulations, treating the electrosprayed solution as leaky dielectric fluid, to address the influence of bulk conductivity and applied potential difference on the developing cone-jet morphology and stability, and to confirm and assist in explaining the experimental trends. In the present, exclusively experimental work we build on our earlier conclusions and substantially extend the previous data set by providing a comprehensive cone-jet stability analysis for the electrosprayed solutions, including the applicable range of potential differences, different formic acid contents, the most relevant aqueous-organic solvent mixtures in RP-HPLC (from 0 to 100% organic modifier content), and different flow rates in the nano-ESI-MS regime. As the electrospray characteristics strongly depend on a number of parameters, the direct transfer of our results to other microchip-HPLC/ESI-MS configurations is difficult, but the general trends reported in this work will assist in a better understanding of the instabilities observed during HPLC/ESI-MS analysis.

2. Experimental

2.1. Microchip electrospray configuration and analysis

We used an Agilent HPLC-Chip-Cube MS interface with a HPLC-MS microchip coupled to a 1200 LC/MSD XCT Ultra ion trap mass spectrometer (Agilent Technologies, Waldbronn, Germany). The polyimide-based microchip [35,36] contains a 6-port valve for mobile phase and sample injection, two particle-packed microchannels that serve as sample enrichment (U-shaped) and separation column (straight), and a nanoelectrospray tip; an integrated interface provides the electrical contact to the liquid at *ca.* 6 mm distance from the chip outlet, within a narrow transfer channel between separation column and nanoelectrospray tip (Fig. 1A). The tip has an outer diameter of *ca.* 45 μm and a Gaussian-shaped opening of *ca.* 15 μm height (Fig. 1B).

The HPLC-MS microchip was positioned inside the chip-cube spray chamber between a counter electrode (end cap of the MS) and an additional electrode, 90° off-axis with respect to the MS inlet cone such that the ESI tip was *ca.* 3 mm away from the cone and *ca.* 3.5 mm above its axis (Fig. 1C). For operation in the positive ion mode, ground potential was applied to the liquid and negative potential to end cap and additional electrode. A constant potential

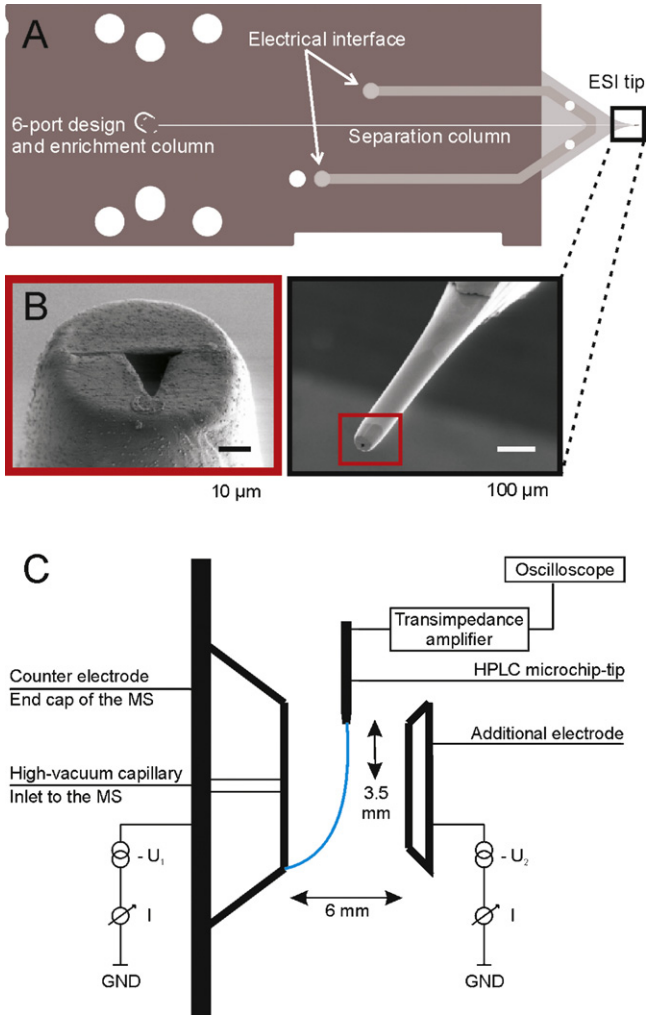

Fig. 1. Layout of the microchip-HPLC/ESI-MS configuration. (A) Polyimide-based microchip with U-shaped sample enrichment column, straight separation column (43 mm long), ESI tip and electrical interface. (B) Magnification of the ESI tip and its outlet. (C) Positioning of the microchip within the ESI-MS interface. Reprinted with permission from Reinsberg et al. [31].

Table 1
Physicochemical properties of the mobile phases [43–45,47–50].

	Water/acetonitrile (v/v)					Water/methanol (v/v)			
	100/0	85/15	45/55	40/60	0/100	85/15	45/55	40/60	0/100
Viscosity [47] (mPa·s)	0.89	0.99	0.77	0.72	0.35	1.29	1.58	1.54	0.56
Density (kg/m^3)	997 [44]	958 [44]	866 [44]	855 [44]	778 [44]	966 [50]	868 [50]	851 [50]	787 [50]
Surface tension (10^{-3} N/m)	70.9 [43]	41.5 [43]	29.8 [43]	29.7 [43]	28.8 [43]	48.5 [48]	27.9 [48]	26.1 [48]	22.5 [48]
Permittivity	78.5 [49]	70.4 [45]	50.8 [45]	48.8 [45]	35.9 [45]	69.7 [49]	45.5 [49]	40.4 [49]	31.5 [49]

difference of 500 V between end cap (U_1) and additional electrode (U_2) made the end cap the part with the most negative potential in the system. Following the settings of the standard Agilent calibration procedure, a drying gas flow rate of 4 L/min and a drying temperature of 300 °C were used.

The potential difference between emitter tip and end cap of the MS was varied *via* the TrapControl software, which allows changes in minimal steps of 50 V. A camera installed in the spray chamber was used to observe the spray performance visually. The electrospray current was measured through the electrical interface on the microchip using a custom-built transimpedance amplifier that converted the incoming current into an outgoing potential difference at 100 nA/V. The transimpedance amplifier was connected (Fig. 1C) to a 10 MHz digital pc-oscilloscope (PicoScope 2204, Pico Technology, St Neots, UK). The oscillosope's Fourier transformation software was used for frequency analysis.

2.2. Mobile phase composition and conductivity measurements

Mobile phases consisted of water and acetonitrile (W/MeCN) or water and methanol (W/MeOH) and contained 0–100 vol% water (Table 1) and 0.001–0.1 vol% formic acid (FA). Acetonitrile and methanol (HPLC grade) were purchased from Sigma–Aldrich Chemie GmbH (Taufkirchen, Germany) and formic acid (*p.a.*) from Fluka-Chemie GmbH (Buchs, Switzerland). HPLC grade water (5.5×10^{-6} S/m) was obtained from a Milli-Q gradient water purification system (Millipore, Bedford, MA, USA).

Conductivity measurements were carried out at room temperature using the Lab 970 conductometer with LF 913T measurement cell from SI Analytics (Mainz, Germany).

3. Results and discussion

3.1. Electrospray mode definitions

There are three major steps in the production of gas-phase ions from the electrolyte ions in solution: (a) production of charged droplets at the electrospray capillary tip; (b) shrinkage of the charged droplets due to solvent evaporation and repeated charge-induced droplet disintegrations leading ultimately to very small highly charged droplets; (c) the actual mechanism by which gas-phase ions are produced from these droplets [16] (and references therein). The electrical field, which is highest near the spray capillary tip, causes the polarization of the solvent near the meniscus of the fluid. In the presence of even traces of an electrolyte the solution will be sufficiently conducting and positive and negative ions will move under the influence of the electrical field. The electromigration leads to an enrichment of positive ions near the liquid–gas interface formed at the capillary outlet in the positive ion mode. The electrical shear stress causes a distortion of the meniscus into an electrified drop growing at the tip or a cone pointing towards the counter electrode. The increase of the liquid's surface is resisted by its surface tension. If the applied field is sufficiently high, the tip becomes unstable and liquid is ejected as a droplet or a fine jet. In the latter case, varicose wave instabilities developing along the surface, lateral kink instabilities, or numerous ramifications cause the jet to break up into charged droplets [17]. The charged droplets are accelerated towards the counter electrode. Solvent evaporation at constant charge leads to droplet shrinkage and an increase of the electric field normal to the surface of the droplets. If the Rayleigh limit is exceeded Coulomb explosion occurs generating smaller droplets, which finally results in ion emission.

Depending on the actual geometrical form taken by the liquid at the capillary outlet (drop, cone), the duty cycle of a liquid ejection, the number, structure (axial, non-axial), and disintegration behavior of the emitted jets, the resulting shapes, sizes, and size distributions of the generated droplets, and the relation between applied potential difference between capillary outlet and counter electrode and resulting spray current, different electrospray modes and regimes can be classified. Confronted with a lack of consensus for the nomenclature of spray modes we chose to follow the classification by Juraschek and Röllgen [27], because they differentiate four distinct spray modes by criteria that could be precisely determined with our instrumental setup. Axial spray mode 1 occurs at lower capillary potentials and features a regular appearance of peak groups in the oscillogram. Axial spray mode 2 is identified by a constant frequency, amplitude, and peak shape of the current pulses (pulsating cone-jet mode). Axial spray mode 3 is characterized by a constant current in the oscillogram and a uniform appearance of the whole liquid cone (cone-jet mode). Beyond a critical value of the capillary potential, the nonaxial regime (spray mode 4) with ejection of multiple jets sets in.

3.2. Experimental analysis of electrospray modes

Figs. 2 and 3 document the four electrospray modes observed for a mobile phase of 60/40 (v/v) W/MeCN with 0.001% FA at a flow rate of 0.3 μL/min, while the potential difference between microchip emitter tip and end cap of the MS was increased from

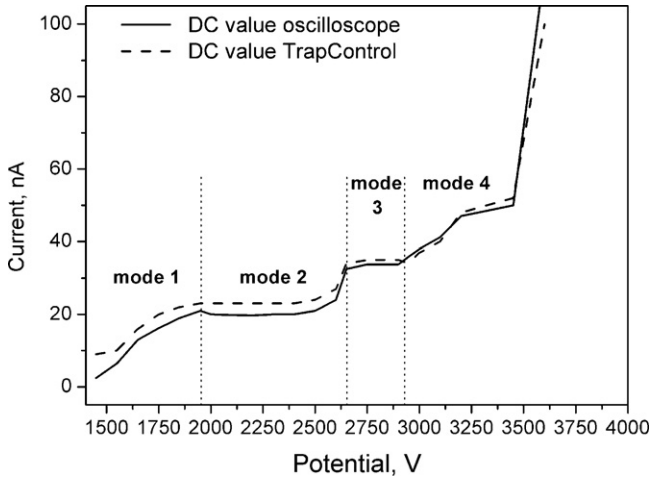

Fig. 2. Microchip emitter current *vs.* applied electrical potential at the end cap of the mass spectrometer's inlet. Mobile phase: 60/40 (v/v) W/MeCN with 0.001% FA, flow rate: 0.3 μL/min. The solid line denotes the DC values detected with the oscilloscope, the dashed line the DC values recorded by the TrapControl software. Changes in slope indicate transitions between individual electrospray modes.

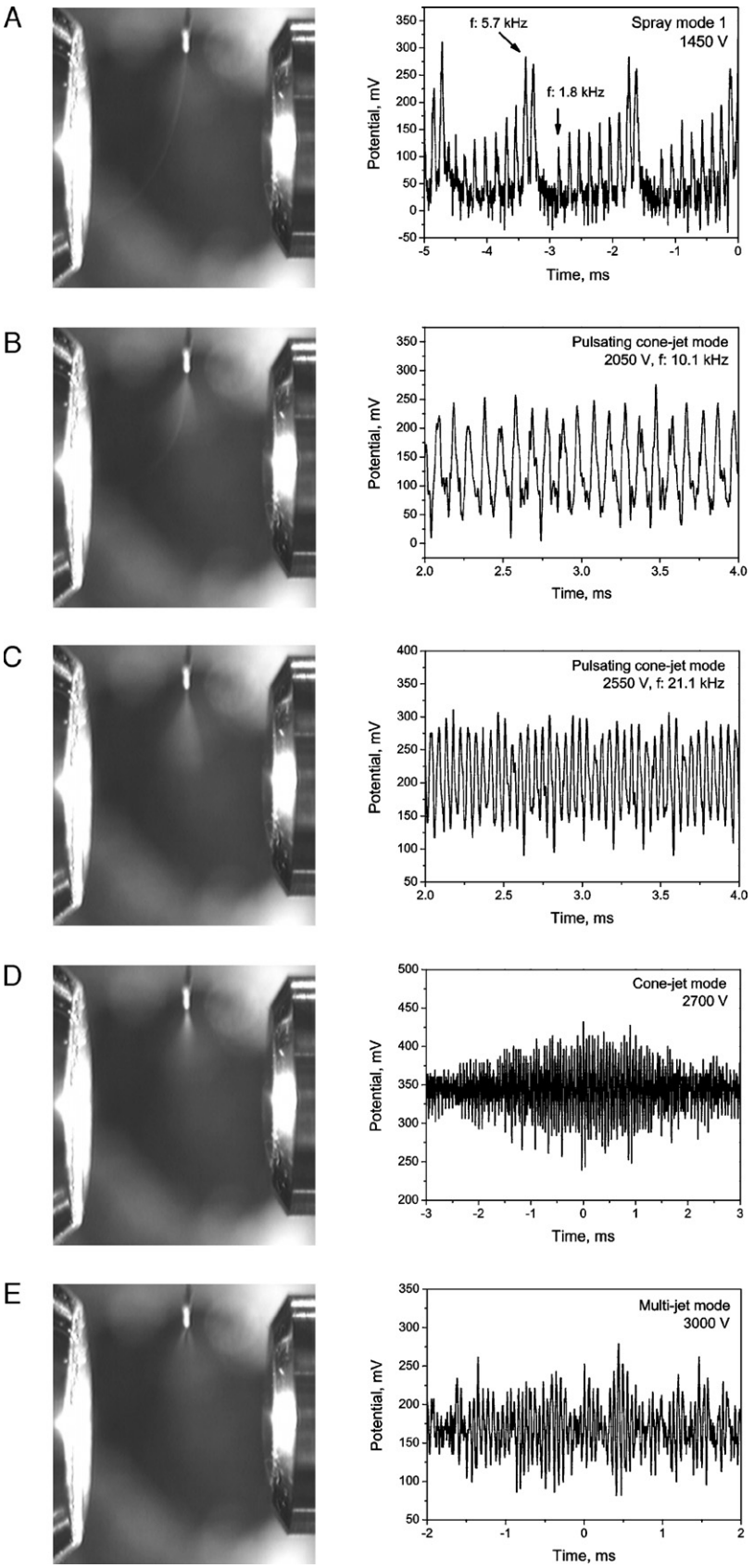

Fig. 3. Analysis of the four observed electrospray modes at increasing potential difference between microchip emitter and end cap of the mass spectrometer by visualization of the spray (left column) and detection of the emitter current *via* the oscilloscope (right column). Mobile phase: 60/40 (v/v) W/MeCN with 0.001% FA, flow rate: 0.3 μL/min. (A) Spray mode 1, potential difference: 1450 V, oscillation frequency: 1.8–5.7 kHz. (B) Spray mode 2 (pulsating cone-jet), 2050 V, 10.1 kHz. (C) Spray mode 2, 2550 V, 21.1 kHz. (D) Spray mode 3 (cone-jet), 2700 V. (E) Spray mode 4 (multi-jet), 3000 V. The corresponding Fourier spectra of the oscillograms can be found in Fig. S1 in the supplementary information of the online version.

1450 to 3600 V. Fig. 2 records the capillary current – the values recorded by the TrapControl software as well as those calculated from the DC component measured by the oscilloscope – as a function of the applied potential. The differences between TrapControl and oscilloscope-based curves are due to rounding errors: the TrapControl software considers only two decimal places, whereas the oscilloscope rounds to the third decimal place. Fig. 3 provides images from the camera in the spray chamber alongside the corresponding oscillograms. At 1450 V (Figs. 2 and 3A) a stream of fluid from the emitter tip is accelerated towards the end cap. Several separated signals at frequencies in the lower kHz range (1.8–5.7 kHz) appear in the associated oscillogram, reflecting polydisperse droplets (mode 1).

Between 1450 and 1950 V the DC current shows Ohmic behavior (Fig. 2), as has also been observed by others [21,27]; the number of observed frequencies decreases and the frequencies are shifted towards higher values. At 2000 V, as the pulsating cone-jet mode sets in, the slope changes abruptly (Fig. 2) and the current remains constant over the next range of potential differences [21]. Current oscillations are regular with a well-defined, principal frequency of 10.1 kHz. The camera captures a less pronounced stream line surrounded by a distinct plume (Fig. 3B). At 2550 V (Fig. 3C), the frequency of the current oscillations increases to 21.1 kHz, which indicates shrinking droplets and ejection at a higher duty cycle [22,29]. While the camera monitors a plume without a visible stream line, the stable DC current as well as the presence of one principal frequency put the region between 2000 and 2550 V firmly into the pulsating cone-jet mode. This example shows that visual inspection of the spray using a camera of a low exposure time and magnification is not adequate to determine the spray mode.

Further increase of the applied voltage leads to a sudden jump in the capillary current (Fig. 2) and a distinct change in oscillogram and spray appearance (Fig. 3D): The oscillogram becomes indistinguishable from the background noise pattern and liquid is ejected as a jet from the apex of a steady cone at the exit of the ESI tip (cone-jet mode, mode 3). The jet subsequently breaks up into smaller droplets due to varicose wave instabilities developing along its surface [17]. To establish the Taylor cone the electrical relaxation time must be shorter than the characteristic time of the liquid supply (the hydrodynamic time). The electrical relaxation time can be calculated according to $t_e = \varepsilon_r/K$, where ε_r is the relative permittivity and K the conductivity of the electrosprayed solution. The hydrodynamic time is given by $t_h \sim L/U$ with the characteristic dimension L and the fluid velocity U [37]. The stable capillary current in the cone-jet mode is explained by the constant generation rate of monodisperse, charged droplets [38]. The current emitted from a Taylor cone is independent from the applied voltage and higher than the current in the pulsating cone-jet mode due to a higher duty cycle [27,39]. Modeling the morphology of a Taylor cone, Reinsberg et al. [31] observed that with increasing applied potential the cone shape transforms from initially convex *via* a straight generatrix to concave. Concomitantly, the cone volume and tip height as well as the jet diameter decrease and the jet velocity increases as the upper voltage-boundary of the cone-jet stability island is approached.

Above 2950 V the axial cone disappears in favor of two jets at opposite sides relative to the axis (Fig. 3E). The capillary current becomes an increasing function of the potential difference (Fig. 2) and oscillates irregularly, so that Fourier analysis revealed no principal frequency. It can reasonably be assumed that each jet emerges with a different pulsation frequency, which would explain the absence of well-defined peaks in the Fourier spectra. At 3450 V the plume of each jet opens up, resulting in a steep rise of the capillary current (Fig. 2). Operating the microchip at capillary currents >100 nA decreases its lifetime significantly, which is why we usually stopped our experiments at this limit unless otherwise indicated.

3.3. Flow-rate dependence of the cone-jet stability island

The flow-rate dependence of the cone-jet stability island [40] has been investigated for various emitters [19,38,41]. The flow rate affects size distribution and charge of the droplets [42] and thus the electrospray mode. To quantify the impact of different flow rates on the electrospray stability in our system, we studied a flow-rate range of 0.1–0.8 μL/min for four mobile phase compositions. Fig. 4A and B compare the effects of 0.001% and 0.1% FA, respectively, in a mobile phase of 45/55 (v/v) W/MeCN. The conductivity of the 0.1% FA-containing W/MeCN mixture is approximately ten times higher (86.6 μS/cm) than those of the 0.001% FA-containing W/MeCN mixture (8.8 μS/cm). Because we are primarily interested in the cone-jet stability island, modes 1 and 2 were condensed to simplify the figures. The onset potentials of mode 1 are very similar for both FA concentrations (2200 and 2300 V), because mode 1 depends not only on electrical forces and conductivity, but also on gravity, liquid pressure, and surface tension. A large difference exists between the two FA concentrations for the electrical potential at which the current limit of 100 nA over the microchip is reached: 3600 V for the low-FA, low-conductivity mixture (Fig. 4A) and *ca.* 2400 V for the high-FA, high-conductivity mixture (Fig. 4B).

The cone-jet regime of the 0.1% FA-containing W/MeCN mixture is shifted to lower flow rates (0.25–0.35 μL/min) and smaller electrical potentials and its stability island is smaller than that of the 0.001% FA-containing W/MeCN mixture, which covers a range of 0.3–0.5 μL/min. At higher flow rates the primary emitted droplets become too large for the development of a stable cone-jet. The shift towards lower flow rates of the cone-jet mode for the high-conductivity mixture (Fig. 4B) can be explained by a faster charge migration inside the solution towards the liquid–gas interface and a shorter electrical relaxation time [42]. The conical meniscus that develops when capillary, hydrostatic, and electrostatic pressures are in equilibrium at each point of the surface [40] is less perturbed and stabilizes the cone-jet mode at lower flow rates.

Fig. 4C and D display the electrospray stability diagrams for 45/55 (v/v) W/MeOH with 0.001% FA (Fig. 4C) or 0.1% FA (Fig. 4D). The trends are the same as observed for the W/MeCN mixtures: When the conductivity of the mobile phase is increased, the cone-jet stability island shrinks and is shifted towards lower flow rates and electrical potentials. Compared with the corresponding W/MeCN mixtures, the cone-jet stability island of the W/MeOH mixtures is larger and stretched towards lower flow rates and electrical potentials. For development of a stable cone-jet, the electrical relaxation time t_e must be small compared with the hydrodynamic time t_h. If t_h approaches t_e, the charge layer on the cone surface is no longer relaxed, and the jet break-up causes large electrohydrodynamic perturbations leading to a dripping or pulsating cone-jet mode (modes 1 and 2). The conductivities of the W/MeOH mixtures are higher than those of the corresponding W/MeCN mixtures (12.1 *vs.* 8.8 μS/cm and 133.4 *vs.* 86.8 μS/cm, for 0.001% and 0.1% FA, respectively, *cf.* Fig. 5). The higher conductivities of the W/MeOH mixtures enhance the difference between electrical relaxation and hydrodynamic time at low flow rates, which is why their cone-jet stability islands cover a broader flow-rate range. For the 0.001% FA-containing mixtures, the cone-jet stability island of the W/MeOH mixture extends that of the W/MeCN mixture by 0.05 μL/min on each side (Fig. 4A and C). For the 0.1% FA-containing mixtures, the cone-jet regime of the W/MeOH mixture stretches down to a flow rate of 0.1 μL/min, whereas a stable cone-jet is not observed below a flow rate of 0.25 μL/min for the W/MeCN mixture (Fig. 4B and D).

Fig. 3 shows that a transition between the different spray modes can be easily induced by changing the applied voltage. Conversely,

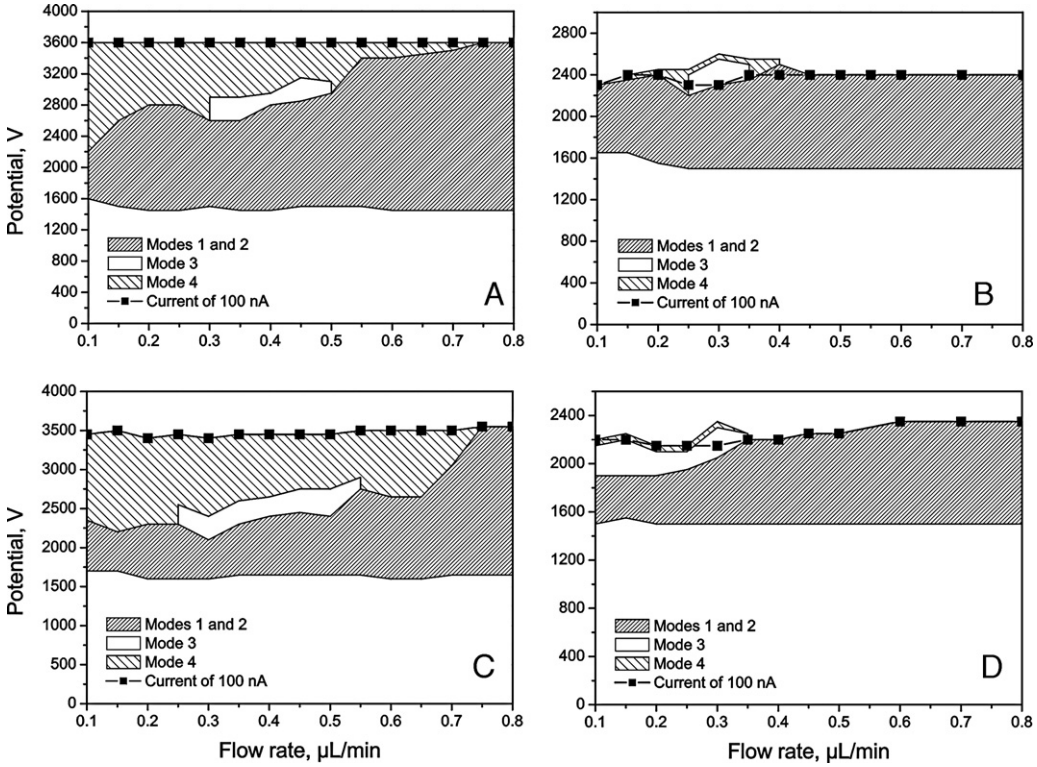

Fig. 4. Flow-rate dependence of the cone-jet stability island for various mobile phase compositions: (A) 45/55 (v/v) W/MeCN, 0.001% FA; (B) 45/55 (v/v) W/MeCN, 0.1% FA; (C) 45/55 (v/v) W/MeOH, 0.001% FA; (D) 45/55 (v/v) W/MeOH, 0.1% FA.

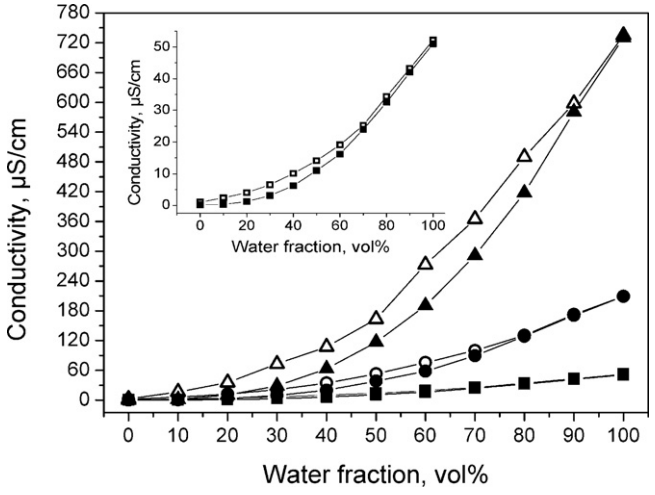

Fig. 5. Experimentally determined electrical conductivities of W/MeCN and W/MeOH mobile phases containing varying amounts of FA. (■) W/MeCN, 0.001% FA; (●) W/MeCN, 0.01% FA; (▲) W/MeCN, 0.1% FA; (□) W/MeOH, 0.001% FA; (○) W/MeOH, 0.01% FA; (△) W/MeOH, 0.1% FA.

at constant voltage the spray mode can be influenced by changing the mobile phase properties and flow rates. If a high backpressure from the chromatographic column enforces a reduced system flow rate, increasing the conductivity of the mobile phase (by adding a higher amount of acid or changing the organic modifier from MeCN to MeOH) could help to achieve a stable cone-jet.

3.4. Influence of water fraction and formic acid content

A decreasing water fraction in the mobile phase is generally accompanied by a decrease in bulk conductivity (Fig. 5), surface tension, permittivity, and density (Table 1) of the electrosprayed solution. Fig. 6A–C show the electrospray characteristics for W/MeCN mobile phases containing 0–100% water and 0.001% (Fig. 6A), 0.01% (Fig. 6B), or 0.1% FA (Fig. 6C) at a flow rate of 0.3 μL/min. In all cases, the onset potentials of mode 1 increase from 0 to 100% water, because of the exponential increase of the surface tension with the water fraction in the mobile phase (*cf.* Table 1 and Ref. [43]). Density and permittivity of the mobile phase (with nearly linear dependence on the water fraction [44,45]) play a minor role, as otherwise the onset potentials would decrease with increasing water fraction. The electrical potential for the current limit of 100 nA over the microchip is a decreasing function of the conductivity and water fraction of the mobile phase (Fig. 6A–C). W/MeCN mixtures with 0.001% FA have a stable cone-jet at 42–86% water (Fig. 6A). This remains essentially unchanged for 0.01% FA (stable cone-jet for 40–85% water), but here the potential for the current limit is shifted towards lower values due to the higher conductivity of the solution (Fig. 6B). The cone-jet stability island thus exceeds the current limit for water fractions >65%. Operating in the cone-jet mode under these conditions would alter the nozzle and degrade the lifetime of the microchip. In Fig. 6C, the effect of the mobile phase conductivity on the electrospray characteristics is more pronounced. For a mobile phase of 85/15 (v/v) W/MeCN, for example, the conductivity changes from 37 μS/cm at 0.001% FA to 150 μS/cm at 0.01% FA (Fig. 5), a change that the cone-jet mode tolerates. But a further increase to 0.1% FA raises the conductivity of the mobile phase to 495 μS/cm, a value that precludes the formation of a stable cone-jet in our instrumental setup (Fig. 6C). Consequently, the cone-jet region for W/MeCN mixtures with 0.1% FA is shifted towards lower water fractions and confined to a range of 22–50% water. However, the current limit is already reached at 43% water.

If the lower limit of the cone-jet stability island is expressed in terms of the mobile phase conductivity, the values for different amounts of FA are very similar: the lower limit for W/MeCN mixtures is at bulk conductivities between 10 and 20 μS/cm (*cf.* Fig. 5).

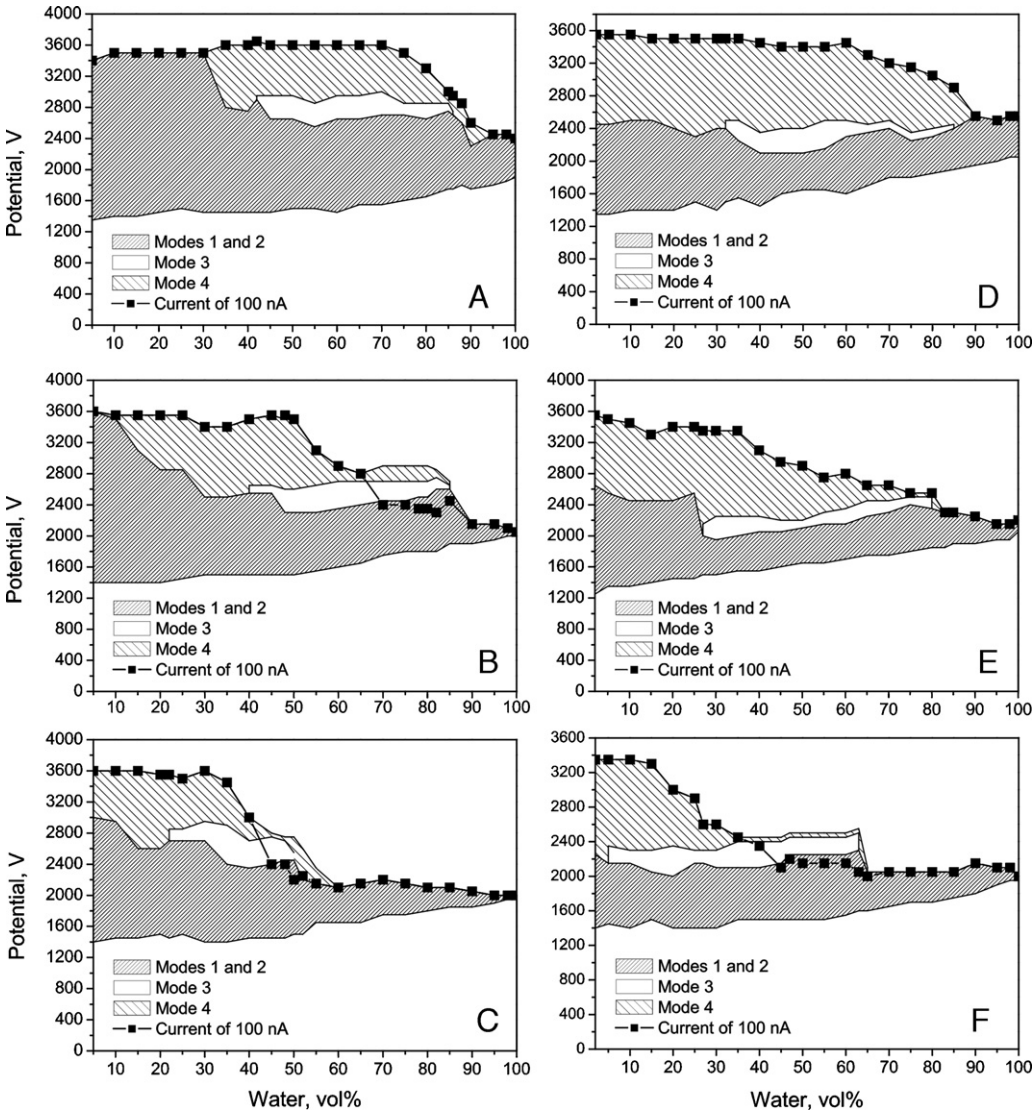

Fig. 6. Electrospray characteristics for different mobile phase compositions at a flow rate of 0.3 μL/min. (A) W/MeCN, 0.001% FA; (B) W/MeCN, 0.01% FA; (C) W/MeCN, 0.1% FA; (D) W/MeOH, 0.001% FA; (E) W/MeOH, 0.01% FA; (F) W/MeOH, 0.01% FA.

Below this limit, at bulk conductivities <10 μS/cm, the droplet generation rate is very slow compared with the acceleration of the charged droplets towards the counter electrode, which results in an oscillating spray current. Thus, for W/MeCN mixtures with 0.001% FA only mode 1 can be generated at water fractions <35%.

A stable cone-jet was not observed for solutions of 0.001%, 0.01%, or 0.1% FA in neat water before the current limit was reached. The difficulty of electrospraying water without organic modifier is well known. The threshold of the critical electrical field required to form a stable cone-jet increases with the surface tension of the liquid–gas atmosphere [46]. Before this value is reached for water, spontaneous corona discharges can be initiated at the capillary outlet [17].

The conductivities of W/MeOH are higher than those of W/MeCN mixtures (Fig. 5). Yet the limiting electrical potentials (currents > 100 nA) for W/MeOH mixtures (Fig. 6D–F) are only partly below those of W/MeCN mixtures (Fig. 6A–C), because the higher viscosity and surface tension of W/MeOH solutions (*cf.* Table 1 and Refs. [43,47,48]) counteract the effect of conductivity. The actual value of the emitter current depends on the distance between emitter tip and counter electrode and their vertical arrangement. Droplets from a high-viscosity liquid do not directly hit the counter electrode, but describe a longer trajectory. The additional distance covered by the charged droplets decreases the emitter current. This effect is observed for W/MeOH with 0.01% FA (Fig. 6E), where the stable cone-jet regime is below the current limit, as opposed to the corresponding W/MeCN mixture (Fig. 6B), for which the stable cone-jet region extends above the current limit at 70–85% water.

The onset potentials of mode 1 are again very similar for all investigated mobile phase compositions and conductivities, because they are mainly determined by liquid pressure, gravitational force, and surface tension. The cone-jet stability regions for W/MeOH mixtures extend over a broader range towards lower water fractions and their onset potentials are smaller than those of the W/MeCN mixtures. This is explained by the higher conductivity of W/MeOH mixtures (Fig. 6D–F): expressed in conductivity values, the lower limits for a stable cone-jet agree well with the 10–20 μS/cm found for W/MeCN (Fig. 5).

The upper cone-jet limit of W/MeOH mixtures is found at conductivities of 39 μS/cm (0.001% FA), 130 μS/cm (0.01% FA), and 300 μS/cm (0.1% FA). The upper cone-jet limits of the mobile phases with 0.001% and 0.01% FA are at 85% and 80% water, respectively, close to the limits of their MeCN counterparts at very similar conductivities (Fig. 5) and slightly higher surface tension (*cf.* Table 1 and

Refs. [43,48]). For higher water fractions mode 2 directly transcends into mode 4 without going through a cone-jet phase (Fig. 6A and D). This behavior can be explained by the parameters that influence cone shape and height. With increasing field strength the jet formation zone extends further towards the base of the cone, yielding a rather concave shape [31], until it begins at the capillary outlet. This situation is unstable, and two jets at opposite sides relative to the axis are ejected from the rim of the capillary [26]. The meniscus is still very flat, with only short cones at the emission points. At high water fractions, surface tension and permittivity increase (*cf.* Refs. [43,45,48,49]). The surface tension raises the threshold of the critical electrical field required to generate a stable cone-jet. An increase in permittivity has the same effect as increasing the applied electrical field: the cone tip height decreases and the acceleration zone extends further towards the cone base. A combination of these effects destabilizes the cone-jet and leads to the transition into a multi-jet region foregoing a stable cone-jet between the pulsating cone-jet and the multi-jet regime. A high conductivity of the mobile phase counteracts these effects. The cone morphology is elongated with a relatively large volume and a convex shape [31]. The jet formation zone is limited to the apex of the meniscus. The remaining surface is practically equipotential, and an almost static equilibrium of forces exists at each point. From this it would be expected that the cone-jet stability island for mobile phases of higher conductivity should be extended towards higher water fractions. But W/MeOH mixtures with 0.1% FA (Fig. 6F) develop no cone-jet mode for >63% water, and the corresponding W/MeCN mixtures (Fig. 6C) behave similarly, with an upper cone-jet limit at 50% water.

To understand why the cone-jet mode cannot develop for mobile phases containing a high amount of water and FA, the explanations given above must be complemented by specifying some system-dependent parameters that influence the electrospray mode, *e.g.*, the electrode arrangement inside the spray chamber (Fig. 1) and the parameter settings. The emitted jets or droplets are attracted not only by the end cap, but also by the additional electrode. If the liquid jet or at least parts of it is sidetracked towards the additional electrode, it either oscillates between end cap and additional electrode or breaks up into several jets (mode 4). With increasing conductivity, surface tension, and permittivity of the mobile phase, the attractive forces of the additional electrode gain influence. Aside from the changes in the physicochemical properties of the mobile phase and the resulting electrical forces, the cone volume is reduced by evaporation of the liquid due to high temperature and drying gas flow in the interface. With a rather concave cone shape (resulting from an increase in permittivity and applied potential), liquid evaporation is expected to gain influence due to the increased surface-to-volume ratio of the cone. These effects are detrimental to a stable cone-jet and restrict the cone-jet stability island to comparatively low water fractions. Reducing the drying temperature and drying gas flow rate yields a higher fluid volume at the nozzle, which may build up and stabilize the cone.

3.5. Effect of a gradually changing mobile phase conductivity

We studied how a gradual change of the conductivity of the mobile phase would alter the electrospray behavior by varying the amount of FA from 0.001% to 0.1% in mixtures of 85/15 (v/v) W/MeCN and 40/60 (v/v) W/MeCN (Fig. 7A and B, respectively). The chosen volumetric ratios represent typical start and end mobile phase compositions in RP-HPLC gradient elution separations. A water fraction of 85% in W/MeCN mixtures is also the upper limit for the cone-jet mode (*cf.* Fig. 6A and B). The flow rate was kept at 0.3 μL/min, while the potential difference was increased until the stable cone-jet disappeared or the current limit of 100 nA over the microchip was reached. With a mobile phase of 85/15 (v/v) W/MeCN a stable cone-jet can be generated at 0.001–0.01% FA content (Fig. 7A). Within this range of FA concentrations, the onset potential for the cone-jet mode decreases and the range of electrical potentials before the current reaches 100 nA narrows with increasing mobile phase conductivity (Fig. 7A). No stable cone-jet is observed for FA > 0.01% and for FA > 0.03% the electrospray exists only in modes 1 and 2.

With a mobile phase of 40/60 (v/v) W/MeCN (Fig. 7B) the cone-jet mode is shifted to higher amounts of FA. For FA < 0.003% the conductivity is too low for a continuous droplet generation, thus, the resulting electrospray shows oscillating behavior. With increasing conductivity the onset potentials of the cone-jet mode decrease and the operational range of electrical potentials widens.

A comparison of Fig. 7A and B reveals the conditions for maintaining a stable cone-jet during a mobile phase gradient from 85/15 (v/v) to 40/60 (v/v) W/MeCN: a concentration of 0.01% FA and an electrical potential of 2600 V. Setting other conditions a continuous operation in the cone-jet mode during this mobile phase gradient is impossible. A mobile phase gradient starting with a water fraction > 85% (98% is not uncommon) would exceed the microchip's current limit due to the high conductivity of the mobile phase (*cf.* Fig. 6B). The conclusions from Fig. 7 are not only relevant for gradient elution RP-HPLC, where the increasing fraction of organic modifier in the mobile phase effects a gradual change of the bulk conductivity, but also for temporary increases in conductivity, which occur, *e.g.*, during analysis of biological samples that have a higher concentration of ionic species (background salts and analytes) than the running mobile phase.

If the goal is to operate continuously in the cone-jet mode, the experimental parameters have to be adapted during HPLC/MS

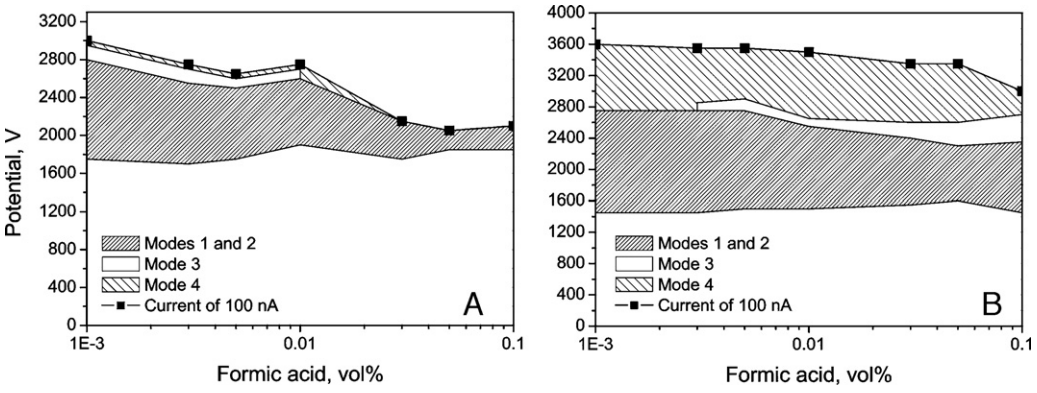

Fig. 7. Electrospray characteristics for bulk conductivity changes of the mobile phase due to an increasing FA content (0.001–0.1%). Mobile phase: (A) 85/15 (v/v) W/MeCN; (B) 40/60 (v/v) W/MeCN. Flow rate: 0.3 μL/min.

analysis to the physicochemical properties of the electrosprayed solution.

4. Conclusions

A commercial microchip-HPLC/ESI-MS configuration was modified for electrospray diagnostics based on frequency analysis of the microchip emitter current and spray imaging. This approach enabled the detection of different spray modes, the cone-jet mode in particular, and their stability regimes under varied experimental conditions. Water–acetonitrile and water–methanol mixtures with formic acid were chosen as the electrosprayed solutions to represent typical mobile phases in RP-HPLC.

At low water fractions in the mobile phase the stability regime is limited by the bulk conductivity: below a critical conductivity the droplet generation rate, which depends on charge separation, is too slow for a stable cone-jet. With increasing bulk conductivity of the mobile phase the cone-jet stability island is shifted towards larger amounts of organic modifier. Due to the higher conductivity of water–methanol compared with water–acetonitrile mixtures, the cone-jet stability islands of water–methanol mobile phases are larger and tolerate higher fractions of organic modifier as well as lower flow rates.

At high water fractions and conductivities, the attractive forces of the additional electrode in our instrumental setup on the liquid jet gain influence so that the cone-jet mode is by-passed and the pulsating cone-jet mode transcends directly into the multi-jet mode. A water fraction > 85% in the mobile phase prevents the generation of a stable cone-jet mode even at moderate bulk conductivities (low amount of formic acid), because of the increased surface tension of the electrosprayed liquid. To counteract at least the destabilizing effect of permittivity, the cone volume can be enlarged by reducing the drying temperature and gas flow in the electrospray interface. Additionally, the current limit for operating the microchip has to be kept in mind, and this limit is shifted to lower water fractions if larger amounts of formic acid or other conductivity-enhancing solvents are present and shrinks the operational range further.

This work demonstrates that during a typical gradient elution HPLC/ESI-MS analysis the cone-jet stability island is easily crossed because of dynamic changes in bulk conductivity and surface tension of the electrosprayed liquid. With a relatively simple modification of the ESI-MS configuration by introducing a transimpedance amplifier and an oscilloscope into the electrical circuit the emitter current provides excellent feedback for electrospray diagnostics. Further investigations of the influence of electrospray instabilities on the performance of HPLC/ESI-MS analyses will assist in the development of hard- and software for online monitoring and controlling the electrospray mode which will irretrievably lead to an improvement of the sensitivity and reproducibility of HPLC-MS methods. Based on the insight gained from our previous work [31] and the comprehensive data set of the present work we are currently implementing an on-line conductivity correction, *i.e.*, a microchip design that is able to compensate the dynamic changes in bulk conductivity during RP-HPLC. Complementary, we will quantify these and accompanying effects on analyte count rates and peak areas as well as their accuracy and repeatability under different electrospray mode conditions.

Acknowledgement

This work was supported by Agilent Technologies through Agilent's University Relations Research Grant program.

Appendix A. Supplementary data

Supplementary data associated with this article can be found, in the online version, at doi:10.1016/j.chroma.2011.01.054.

References

[1] X. Chen, D.-F. Cui, Microsyst. Technol. 15 (2009) 667.
[2] K. Ohno, K. Tachikawa, A. Manz, Electrophoresis 29 (2008) 4443.
[3] I. Oita, H. Halewyck, B. Thys, B. Rombaut, Y. Vander Heyden, D. Mangelings, Anal. Bioanal. Chem. 398 (2010) 239.
[4] D. Mark, S. Häberle, G. Roth, F. von Stetten, R. Zengerle, Chem. Soc. Rev. 39 (2010) 1153.
[5] J.R. Kraly, R.E. Holcomb, Q. Guan, C.S. Henry, Anal. Chim. Acta 653 (2009) 23.
[6] K. Gupta, D.-H. Kim, D. Ellison, C. Smith, A. Kundu, J. Tuan, K.-Y. Suh, A. Levchenko, Lab Chip 10 (2010) 2019.
[7] A. Arora, G. Simone, G.B. Salieb-Beugelaar, J.T. Kim, A. Manz, Anal. Chem. 82 (2010) 4830.
[8] J.F. Dishinger, R.T. Kennedy, Electrophoresis 29 (2008) 3296.
[9] K. Uchiyama, H. Nakajima, T. Hobo, Anal. Bioanal. Chem. 379 (2004) 375.
[10] J. Lee, S.A. Soper, K.K. Murray, J. Mass Spectrom. 44 (2009) 579.
[11] T. Sikanen, S. Franssila, T.J. Kauppila, R. Kostiainen, T. Kotiaho, R.A. Ketola, Mass Spectrom. Rev. 29 (2010) 351.
[12] S. Koster, E. Verpoorte, Lab Chip 7 (2007) 1394.
[13] I.M. Lazar, J. Grym, F. Foret, Mass Spectrom. Rev. 25 (2006) 573.
[14] S. Khirevich, A. Höltzel, D. Hlushkou, U. Tallarek, Anal. Chem. 79 (2007) 9340.
[15] M. Prudent, H.H. Girault, Analyst 134 (2009) 2189.
[16] P. Kebarle, U.H. Verkerk, Mass Spectrom. Rev. 28 (2009) 898.
[17] M. Cloupeau, B. Prunet-Foch, J. Aerosol Sci. 25 (1994) 1021.
[18] R. Kostiainen, T.J. Kauppila, J. Chromatogr. A 1216 (2009) 685.
[19] R.T. Kelly, K. Tang, D. Irimia, M. Toner, R.D. Smith, Anal. Chem. 80 (2008) 3824.
[20] I. Marginean, R.T. Kelly, R.J. Moore, D.C. Prior, B.L. LaMarche, K. Tang, R.D. Smith, J. Am. Soc. Mass Spectrom. 20 (2009) 682.
[21] I. Marginean, R.T. Kelly, D.C. Prior, B.L. LaMarche, K. Tang, R.D. Smith, Anal. Chem. 80 (2008) 6573.
[22] G.A. Valaskovic, J.P. Murphy, M.S. Lee, J. Am. Soc. Mass Spectrom. 15 (2004) 1201.
[23] H. Yin, K. Killeen, J. Sep. Sci. 30 (2007) 1427.
[24] P. Hoffmann, M. Eschner, S. Fritzsche, D. Belder, Anal. Chem. 81 (2009) 7256.
[25] S.L.S. Freire, H. Yang, A.R. Wheeler, Electrophoresis 29 (2008) 1836.
[26] A. Jaworek, A. Krupa, J. Aerosol Sci. 30 (1999) 873.
[27] R. Juraschek, F.W. Röllgen, Int. J. Mass Spectrom. 177 (1998) 1.
[28] I. Marginean, L. Parvin, L. Heffernan, A. Vertes, Anal. Chem. 76 (2004) 4202.
[29] P. Nemes, I. Marginean, A. Vertes, Anal. Chem. 79 (2007) 3105.
[30] L. Parvin, M.C. Galicia, J.M. Gauntt, L.M. Carney, A.B. Nguyen, E. Park, L. Heffernan, A. Vertes, Anal. Chem. 77 (2005) 3908.
[31] K.-G. Reinsberg, U. Effelsberg, U. Tallarek, Lab Chip 9 (2009) 2914.
[32] A. Gapeev, A. Berton, D. Fabris, J. Am. Soc. Mass Spectrom. 20 (2009) 1334.
[33] R. Ramanathan, R. Zhong, N. Blumenkrantz, S.W. Chowdhury, K.B. Alton, J. Am. Soc. Mass Spectrom. 18 (2007) 1891.
[34] G.O. Staples, H. Naimy, H. Yin, K. Kileen, K. Kraiczek, C.E. Costello, J. Zaia, Anal. Chem. 82 (2010) 516.
[35] S. Ehlert, L. Trojer, M. Vollmer, T. van de Goor, U. Tallarek, J. Mass Spectrom. 45 (2010) 313.
[36] S. Jung, A. Höltzel, S. Ehlert, J.-A. Mora, K. Kraiczek, M. Dittmann, G.P. Rozing, U. Tallarek, Anal. Chem. 81 (2009) 10193.
[37] A.M. Gañán-Calvo, J. Dávila, A. Barrero, J. Aerosol Sci. 28 (1997) 249.
[38] I. Marginean, R.T. Kelly, J.S. Page, K. Tang, R.D. Smith, Anal. Chem. 79 (2007) 8030.
[39] J. Fernández de la Mora, I.G. Loscertales, J. Fluid Mech. 260 (1994) 155.
[40] M. Cloupeau, B. Prunet-Foch, J. Electrostat. 22 (1989) 135.
[41] A. Schmidt, M. Karas, T. Dülcks, J. Am. Soc. Mass Spectrom. 14 (2003) 492.
[42] L. de Juan, J. Fernández de la Mora, J. Colloid Interface Sci. 186 (1997) 280.
[43] W.R. Melander, Cs. Horváth, High Performance Liquid Chromatography – Advances and Perspectives, Academic Press, New York, 1980.
[44] C. Moreau, G. Douhéret, Thermochim. Acta 13 (1975) 385.
[45] C. Moreau, G. Douhéret, J. Chem. Thermodyn. 8 (1976) 403.
[46] J.M. López-Herrera, A. Barrero, A. Boucard, I.G. Loscertales, M. Márquez, J. Am. Soc. Mass Spectrom. 15 (2004) 253.
[47] H. Colin, J.C. Diez-Masa, G. Guiochon, T. Czajkowska, I. Miedziak, J. Chromatogr. 167 (1987) 41.
[48] G. Vázquez, E. Alvarez, J.M. Navaza, J. Chem. Eng. Data 40 (1995) 611.
[49] G. Åkerlöf, J. Am. Chem. Soc. 54 (1932) 4125.
[50] S.Z. Mikhail, W.R. Kimel, J. Chem. Eng. Data 6 (1961) 533.